Journal of Structural Geology 96 (2017) 161–175

Contents lists available at ScienceDirect

Journal of Structural Geology

journal homepage: www.elsevier.com/locate/jsg

Using magma flow indicators to infer flow dynamics in sills

Lauren Hoyer*, Michael K. Watkeys

Geological Sciences, School of Agricultural, Earth and Environmental Sciences, University of KwaZulu-Natal, Westville Campus, Private Bag X54001, Durban 4000, South Africa

ARTICLE INFO

Article history:
Received 15 September 2016
Received in revised form
31 January 2017
Accepted 9 February 2017
Available online 11 February 2017

Keywords:
Magma flow
Sills
Magma flow indicators
Fabric analysis
Fabric overprinting

ABSTRACT

Fabrics from Anisotropy of Magnetic Susceptibility (AMS) analyses and Shape Preferred Orientation (SPO) of plagioclase are compared with field structures (such as bridge structures, intrusive steps and magma lobes) formed during magma intrusion in Jurassic sills. This is to constrain magma flow directions in the sills of the Karoo Igneous Province along the KwaZulu-Natal North Coast and to show how accurately certain structures predict a magma flow sense, thus improving the understanding of the Karoo sub-volcanic dynamics. The AMS fabrics are derived from magnetite grains and are well constrained, however the SPO results are commonly steeply inclined, poorly constrained and differ to the AMS fabrics. Both techniques resulted in asymmetrical fabrics. Successful relationships were established between the AMS fabric and the long axes of the magma flow indicators, implying adequate magma flow prediction. However, where numerous sill segments merge, either in the form of magma lobes or bridge structures, the coalescence process creates a new fabric between the segments preserving late-stage magma migration between the merged segments, overprinting the initial magma flow direction.

1. Introduction

Knowing magma flow directions in sills can provide information about the feeder system and magma migration in the upper crust (Thomson and Hutton, 2004; Hutton, 2009; Schofield et al., 2012a; Magee et al., 2016a). Along the North Coast of KwaZulu-Natal (KZN), South Africa, numerous thin sills (<10 m) crop out as part of the Karoo Igneous Province (KIP), which comprises voluminous continental flood basalts and an extensive sub-volcanic network of dykes and sills (Erlank, 1984). The KIP magmatic event occurred ~183–174 Ma (Jourdan et al., 2005, 2007) with the sills in the main Karoo Basin intruded between 183.0 ± 0.5–182.3 ± 0.6 Ma (Svensen et al., 2012). Field structures (*e.g.* bridge structures, intrusive steps, magma lobes and deformed vesicles) occur in association with the sills, either through magma-host rock interactions or magmatic processes, which can be used to indicate magma flow. These structures have previously been used to define magma flow regimes of both dykes (*e.g.* Pollard et al., 1975; Pollard, 1987; Rickwood, 1990; Liss et al., 2002; Philpotts and Philpotts, 2007) and sills/inclined sheets (*e.g.* Nicholson and Pollard, 1985; Schofield et al., 2012b; Hutton, 2009; Magee et al., 2016a).

Magma flow within small tabular intrusions has been inferred using fabrics techniques including Anisotropy of Magnetic Susceptibility (AMS) and Shape Preferred Orientation (SPO) analyses (*e.g.* Khan, 1962; Ellwood, 1978; Knight and Walker, 1988; Poland et al., 2004; Aubourg et al., 2008). AMS results are often supplemented with petrographic analysis such as SPO studies, increasing the confidence of the inferred flow direction (*e.g.* Launeau and Robin, 1996; Launeau and Cruden, 1998; Horsman et al., 2005; Hastie et al., 2011).

The aim of this study is to elucidate how adequately magma flow indicators can predict magma flow dynamics in sills. This is achieved by (1) observing structures in the field; (2) analysing SPO and AMS fabrics along the sill contacts and inferring magma flow within the sills; (3) comparing the magma flow directions inferred from the field structures with these fabrics. Similar studies have been undertaken on certain aspects of magma flow indicators within sills (*e.g.* Horsman et al., 2005), dykes (*e.g.* Philpotts and Philpotts, 2007) and lava flows (*e.g.* Loock et al., 2008).

2. Geological setting

The Jurassic-aged Karoo dolerite sills belong to an 8 km stretch of coastline along the KZN North Coast, South Africa (Fig. 1). The intrusions differ in scale from the sills in the main Karoo Basin, which are commonly >20 m thick and laterally extensive. Magma

* Corresponding author.
E-mail address: lauren_hoyer@hotmail.com (L. Hoyer).

http://dx.doi.org/10.1016/j.jsg.2017.02.005
0191-8141/

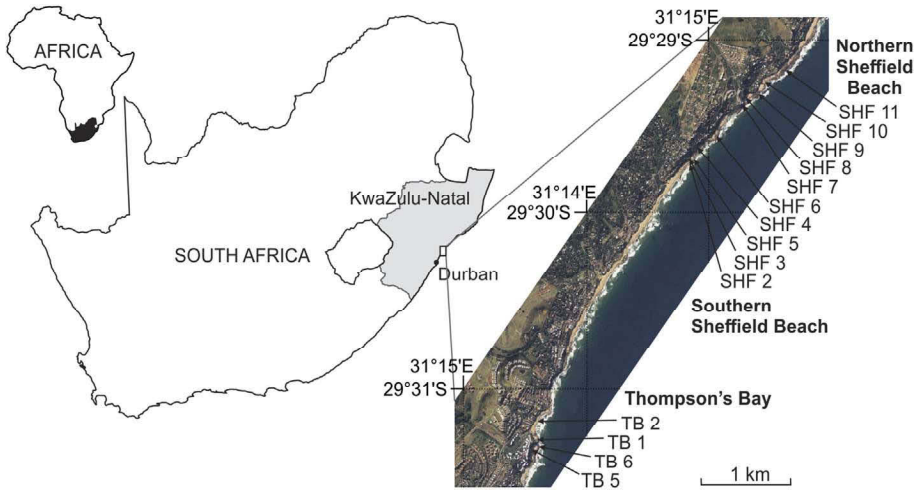

Fig. 1. Locality of the study area along the KwaZulu-Natal North Coast, South Africa. The 14 sills analysed here are named according to the area Thompson's Bay (TB) in the south and Sheffield Beach (SHF) in the north.

flow dynamics and magnetic characteristics have been studied in certain large sills in the basin (*e.g.* Férre et al., 2002; Maes et al., 2008) but no work has been undertaken on the numerous intrusions along the KZN coast. The dolerites intrude Permian age sedimentary rocks of the Vryheid Formation of the Karoo Supergroup, ranging from thinly laminated shales to coarse sandstones. The study area comprises the beaches of Thompson's Bay (TB) and Sheffield Beach (SHF) the latter being further divided into Southern and Northern area. The sills range in thickness from 0.5 m to >6 m (Table 1) and are faulted and tilted by a series of brittle events related to the breakup of Gondwana, which commenced subsequent to the completion of the KIP event (Watkeys, 2006).

3. Recognising magma flow indicators in the field

Where macroscopic fabrics are evident in the form of preferentially aligned coarse crystals along sill contacts, the magma flow direction may be indicated in the field, however thin intrusions typically comprise fine-grained crystals and therefore small-scale imbrications (Blanchard et al., 1979; Rickwood, 1990). Exsolved

Table 1
Field observations and AMS results from Thompson's Bay and Sheffield Beach.

Sill	Orientation		Thickness	MFI Long Axis[a] [b]	Contact	n	Km (10^{-3} SI)	K1[a]	K2[a]	K3[a]	P′ (10^{-3})	T (10^{-3})
	strike/dip	Lat/Long						dec/incl	dec/incl	dec/incl		
TB1	172°/22°	29° 31′ 39.05″ S	3	216°	Upper	11	0.77	275°/08°	183°/11°	038°/76°	1.010	0.210
		31° 13′ 41.17″ E										
TB2	167°/21°	29° 31′ 14.69″ S	2.5	304°	Upper	5	0.64	168°/01°	259°/15°	076°/76°	1.016	−0.081
		31° 13′ 42.05″ E		301°	Vesicular	11	0.68	163°/04°	254°/08°	046°/81°	1.018	−0.297
					Lower	5	1.53	157°/39°	343°/51°	249°/03°	1.017	−0.115
TB5	160°/16°	29° 31′ 25.17″ S	2	307°	Upper	8	10.10	268°/07°	177°/09°	034°/79°	1.052	0.325
		31° 13′ 39.03″ E			Lower	5	6.97	277°/04°	185°/27°	013°/63°	1.032	0.234
TB6	164°/13°	29° 31′ 26.04″ S	unknown	205°/212°	Upper	4	7.04	306°/04°	211°/23°	050°/69°	1.021	−0.359
		31° 13′ 41.80″ E									1.005	0.103
SHF2	000°/20°	29° 29′ 43.44″ S	1	004°	Upper	4	1.37	172°/37°	310°/37°	066°/24°		
		31° 14′ 46.68″ E			Lower	9	4.80	275°/02°	185°/07°	020°/83°	1.018	0.003
SHF3	340°/17°	29° 29′ 41.64″ S	2.2	064°/243°	Upper	8	3.30	240°/33°	111°/44°	350°/28°	1.018	−0.300
		31° 14′ 46.93″ E			Lower	10	4.63	213°/30°	314°/18°	070°/54°	1.016	0.014
SHF4	350°/12°	29° 29′ 37.32″ S	1.5	144°	Upper	6	0.79	323°/05°	054°/22°	211°/78°	1.010	0.134
		31° 14′ 49.56″ E			Lower	4	8.20	155°/12°	062°/12°	283°/72°	1.047	0.316
SHF5	353°/10°	29° 29′ 41.28″ S	1.2	354°	Upper	10	2.72	163°/23°	271°/34°	046°/46°	1.057	−0.056
		31° 14′ 48.48″ E			Lower	9	3.31	184°/24°	273°/02°	007°/67°	1.024	0.321
SHF6	013°/13°	29° 29′ 32.64″ S	2.5	201°/243°/324°/041°	Upper	12	7.50	276°/04°	008°/30°	180°/60°	1.011	0.160
		31° 14′ 57.48″ E			Lower	9	8.81	087°/01°	356°/21°	180°/69°	1.011	−0.156
SHF7	056°/10°	29° 29′ 23.64″ S	>6	055°/060°/064°	Upper	9	6.79	294°/02°	204°/13°	031°/77°	1.019	−0.438
		31° 15′ 07.56″ E			Lower	8	6.38	132°/12°	223°/07°	343°/76°	1.018	−0.118
SHF8	088°/09°	29° 29′ 19.32″ S	0.5	212°/215°/217°/224°	Upper	14	1.61	319°/01°	049°/05°	218°/85°	1.046	−0.029
		31° 15′ 10.44″ E		/228°/057°	Lower	21	1.75	104°/12°	194°/01°	288°/79°	1.027	−0.062
SHF9A	065°/13°	29° 29′ 17.88″ S	1.5	059°/325°/343°/346°	Upper	4	0.67	314°/78°	053°/00°	144°/11°	1.003	−0.499
		31° 15′ 14.04″ E			Lower	5	0.81	026°/38°	199°/52°	294°/03°	1.003	0.103
SHF9B				149°/155°/160°/137°	Lower	27	1.63	341°/78°	196°/10°	105°/07°	1.004	0.082
SHF10	059°/10°	29° 29′ 13.92″ S	1	211°/220°	Upper	4	7.05	209°/10°	105°/11°	320°/75°	1.013	−0.165
		31° 15′ 17.28″ E			Lower	10	7.28	197°/04°	106°/11°	308°/78°	1.014	0.029
SHF11	054°/10°	29° 29′ 10.68″ S	1.5	145°	Upper	5	2.33	195°/90°	286°/00°	016°/00°	1.006	−0.438
		31° 15′ 24.48″ E			Lower	11	7.26	042°/26°	134°/04°	231°/64°	1.010	−0.174

[a] Directional readings restored along with sill contact strike/dip.
[b] Strike/plunge direction of magma flow indicator (MFI).

vesicles that coalesce and rise towards the upper contact of an intrusion may be deformed by magma flow, resulting in elongated vesicles, with the long axes parallel to the direction of magma movement (Rickwood, 1990; Liss et al., 2002). In larger vesicles magma movement may shear the chilled crust on the underside of the vesicle creating "ripples" or folds, the magma flow direction implied by the closure direction of the folds (Fig. 2a) (Fink and Fletcher, 1978; Liss et al., 2002).

Sheet intrusions are initially a series of multiple thin, laterally restricted, discrete magma segments that may become continuous sheets through segment linkage (*e.g.* Rickwood, 1990; Hutton, 2009; Schofield et al., 2012b). When the sill segments merge, host rock deformation allows for the increasing volume of intruding magma (Nicholson and Pollard, 1985; Nicholson and Ejiofor, 1987; Hutton, 2009; Schofield et al., 2012a, b). If the sill segments are in the form of magma lobes at the leading edge of the intrusion, magma flow is towards the termination of a magma lobe (Fig. 2b) (Stevenson et al., 2007; Magee et al., 2012, 2016b). With continued magma propagation, these lobes coalesce to form a continuous sheet-like intrusion (Pollard et al., 1975; Rickwood, 1990; Hutton, 2009; Schofield et al., 2012a).

An intrusive step may form when intruding magma segments overlap vertically but not laterally and are typically steeply inclined with possible host rock fluidisation between segments (Fig. 2c) (Pollard et al., 1975; Rickwood, 1990; Schofield et al., 2012a). When sill segments overlap both laterally and vertically during intrusion, bridge structures form, the shape of which is dictated by initially straight or curved fracture propagation paths (Fig. 2d) (Nicholson and Pollard, 1985; Kattenhorn and Watkeys, 1995; Hutton, 2009). Dilation of these fractures by intruding magma may cross-fracture the country rock at inflection points forming a bent or a broken bridge (Nicholson and Ejiofor, 1987; Morris et al., 2008; Hutton, 2009; Muirhead et al., 2012). Separation of the bridge forms a host rock xenolith which is entrained into the intruding magma leaving a bridge stub along the intrusive contact (Fig. 2d) (Hutton, 2009; Schofield et al., 2012a). Fracture linkages and magma flow result in the long axes of bridge structures and intrusive steps forming parallel to primary flow within the intrusion.

4. Methods

4.1. Sample collection and preparation

Samples were obtained 10–15 cm from the upper and lower sill contacts, using a petroleum-powered handheld drill extracting 25 mm diameter cores. Cores were orientated in the field using a core-orientator and a magnetic compass. Single samples were obtained per site, distal to magma flow indicators to avoid fabric abnormalities near these structures. Three mutually perpendicular sections, were thin sectioned for SPO samples (see Hoyer and Watkeys, 2015) and cylinders <25 mm in length were cut for AMS samples.

4.2. Anisotropy of magnetic susceptibility methodology

AMS is a quantitative measure of the alignment of magnetic phases in a rock mass based on the minerals magnetic susceptibility (Tarling and Hrouda, 1993). The orientation and distribution of magnetic grains in a rock can be determined by their response to an induced magnetic field producing a susceptibility ellipsoid whose principal axes are $K1 \geq K2 \geq K3$, thus defining the AMS ellipsoid. Mafic igneous rocks typically contain ferromagnetic Fe oxides such as magnetite. These minerals may be in the state of single domain (SD), pseudo-single domain (PSD) and multiple domain (MD) (Rochette et al., 1999). The AMS fabrics may have three origins (1) shape fabrics where the $K1$ and $K3$ coincide with the long and short axes of the grain respectively, termed "normal" fabrics; (2) SD-grain shape fabric where $K1$ and $K3$ coincide with the short and long axes of the grain respectively, termed "inverse" fabrics (Stephenson et al., 1986; Rochette et al., 1991, 1999; Tarling and Hrouda, 1993); (3) shape fabric of grain clusters giving an AMS which may be "normal" or "inverse".

AMS was first used by Graham (1954) as a method to directly compare AMS to aspects of the rock fabric. Since then AMS became a widely-used method in determining the magnetic fabrics in rocks and is still considered a powerful tool in rock fabric studies (Khan, 1962; Ellwood, 1978; Knight and Walker, 1988; Rochette et al., 1991;

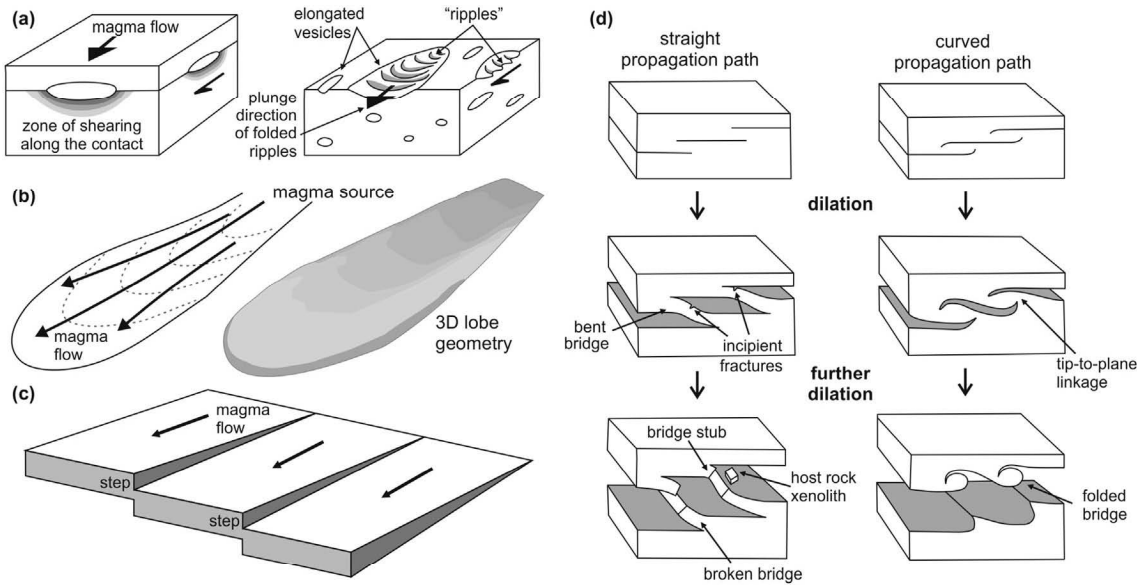

Fig. 2. The formation processes of magma flow indicators. (a) Deformation of the underside of vesicles where a skin of chilled magma around the vesicle becomes sheared resulting in the formation of ropy-flow structures (after Liss et al., 2002). (b) Magma lobes form through dispersive magma flow away from the magma source (after Stevenson et al., 2007). (c) Intrusive steps form through the linkage of magma-filled fractures that overlap laterally (after Pollard et al., 1975; Rickwood, 1990). (d) Bridge structures form through the propagation and dilation of overlapping fractures, bent bridges of country rock form through fracture dilation (after Nicholson and Pollard, 1985; Kattenhorn and Watkeys, 1995).

Tarling and Hrouda, 1993; Ferré et al., 2002; Cañón-Tapia, 2004; Poland et al., 2004; Horsman et al., 2005; Gil-Imaz et al., 2006; Aubourg et al., 2008; Hastie et al., 2011; Magee et al., 2016a). Magnetic mineralogy properties of the magnetic phases are determined using thermomagnetic analyses, to correctly interpret the AMS fabrics, as the mineral properties (*i.e.* domain state) may affect the use of the fabrics as magma flow indicators.

A total of 257 samples were analysed using the AGICO Kappabridge MFK1-FA susceptibility bridge at the Institute for Rock Magnetism at the University of Minnesota using a standard 15 positions procedure (Jelinek, 1978). The results are illustrated using lower hemisphere stereograms with P' (degree of anisotropy) and T (shape parameter) being recorded for each result (Tarling and Hrouda, 1993).

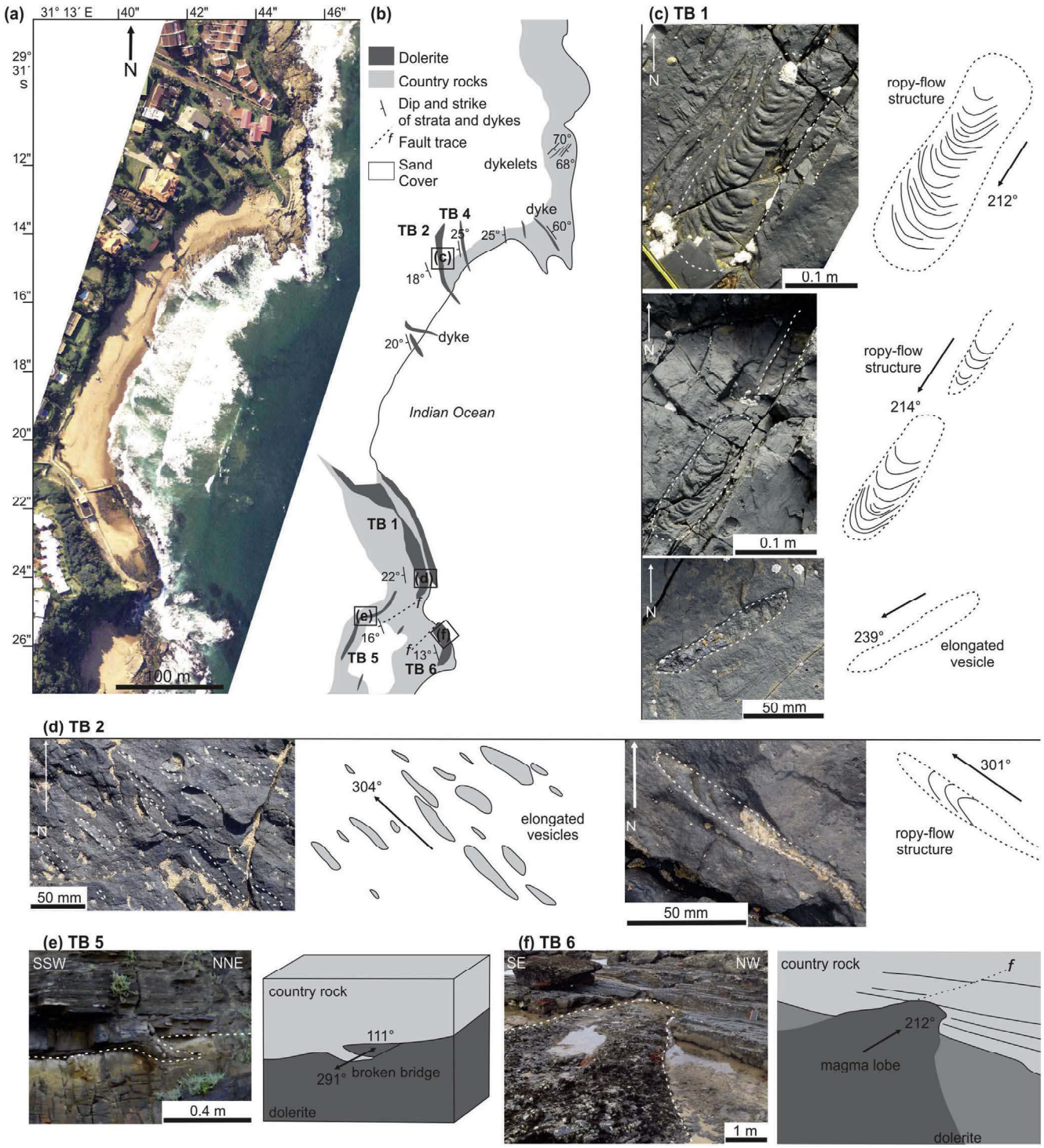

Fig. 3. (a) Aerial photograph and (b) geological map of Thompson's Bay. (c) Ropy-flow structures and elongated vesicles observed below the upper contact of TB1 plunging towards the SW. (d) A ropy-flow structure and elongated vesicles within the vesicular zone of TB2 plunge towards the NE. (e) A broken bridge along the upper contact of TB5 oriented WNW-ESE. (f) A magma lobe along the upper contact of TB6 plunge towards the ~SW.

4.3. Shape-preferred orientation techniques

Defining the SPO is a process of defining the three-dimensional (3-D) shape ellipsoid of a mineral phase, where $L1 \geq L2 \geq L3$. Plagioclase laths were analysed as they were abundant, well-preserved and the only significant colourless mineral present. A total number of 109 samples, giving 327 photomicrographs, were analysed by inverting and filtering the images to extract individual plagioclase grains. SPO-2003 creates 2-D inertia tensor from these images using stacked grain data to define an ellipse (Launeau, 2004; Launeau and Robin, 1996, 2005; Launeau and Cruden, 1998). Three mutually perpendicular 2-D tensors are combined using Ellipsoid-2003 (Robin, 2002; Launeau and Robin, 2005) resulting in a 3-D shape ellipsoid. The shape of the ellipsoid (T) is prolate, triaxial or oblate depending on T being less than, equal to or greater than zero, respectively. An error in the fit of the ellipsoid is measured by the Global Incompatibility Index, $\sqrt{F}$: when $\sqrt{F}$ is zero the ellipse creates a perfect fit (Launeau and Robin, 2005). Results are stereographically projected with 95% confidence ellipses corresponding to a standard deviation of 2.

4.4. Fabrics indicating magma flow

Strain in an inhomogeneous fluid, where the viscosities differ between the particles and the matrix, results in a preferred orientation of the crystals parallel to the direction of flow or shearing (Gay, 1966, 1967; Correa-Gomes et al., 2001; Callot and Guichet, 2003; Cañón-Tapia and Chavez-Alvarez, 2004). Development of crystal imbrications along sill contacts that dip in opposite directions (symmetrical relationship), allow for the magma flow

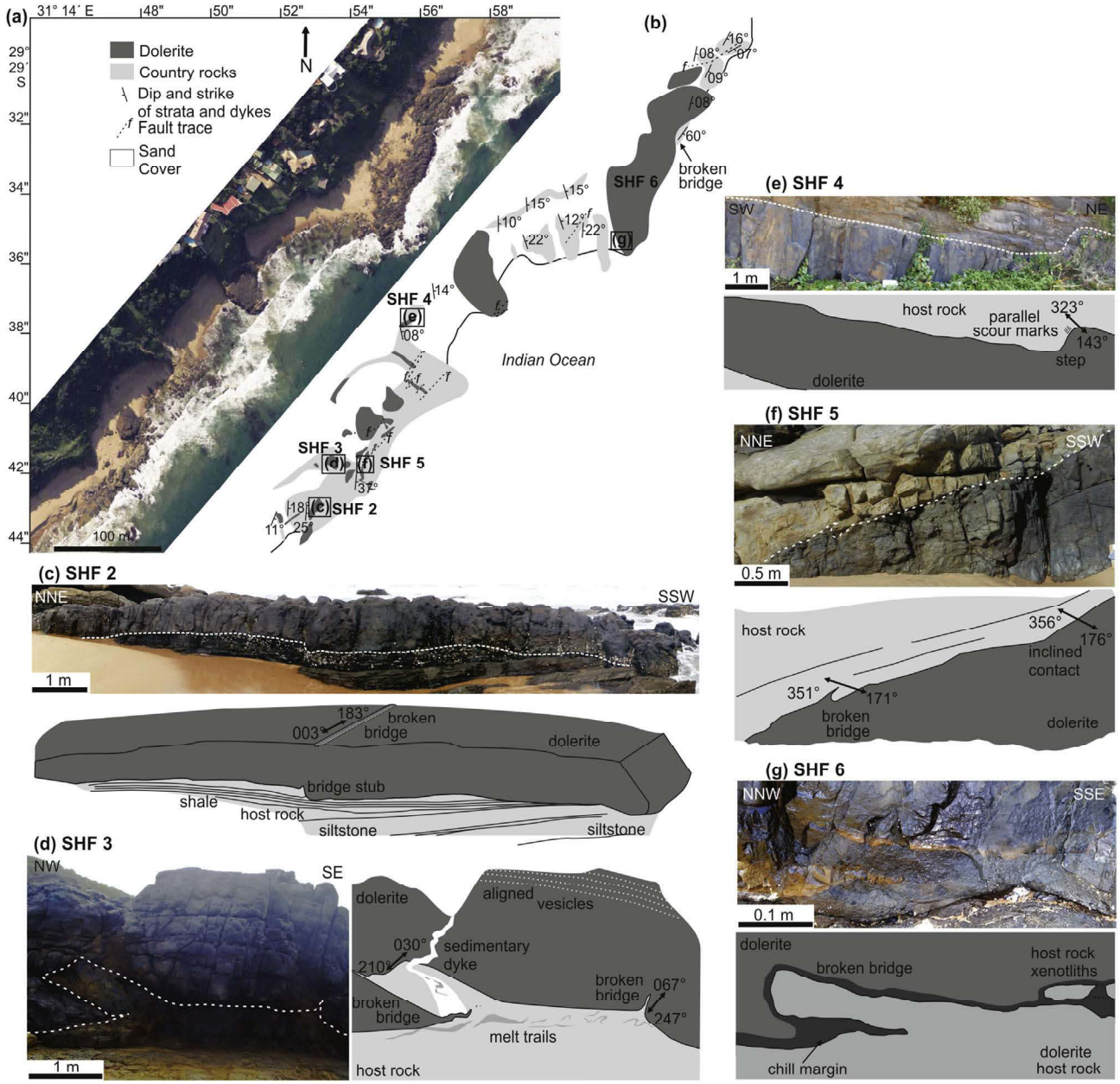

Fig. 4. (a) Aerial photograph and (b) geological map of southern Sheffield Beach. (c) SHF2 has parallel north-south oriented bridge structures along the upper and lower contacts. (d) SHF3 exhibits parallel ENE-WSW oriented bridge structures. (e) An intrusive step occurs in SHF4 with scour marks plunging parallel to the SE — SSE oriented step. (f) SHF5 is a moderately inclined sheet with small ~ N-S oriented bridge structures. (g) SHF6 is intruded into a dolerite sill and has deformed the material along the lower sill contact.

direction to be inferred by the fabric closure direction (Blanchard et al., 1979; Tauxe et al., 1998; Correa-Gomes et al., 2001; Féménias et al., 2004; Gil-Imaz et al., 2006; Magee et al., 2016a). As samples obtained near the chill margins of thin intrusions are likely to represent the initial direction of magma propagation, the acquired fabrics may be a proxy for magma flow (Magee et al., 2016a).

The fabric long axes (lineations), *K*1 for AMS and *L*1 for SPO, have classically been used to define the fabric orientation, as it is assumed that the long axis aligns with the magmatic foliation developed along the intrusive contacts, producing "normal" fabrics (*e.g.* Knight and Walker, 1988; Callot et al., 2001; Liss et al., 2002; Horsman et al., 2005; Morgan et al., 2008). However, in some

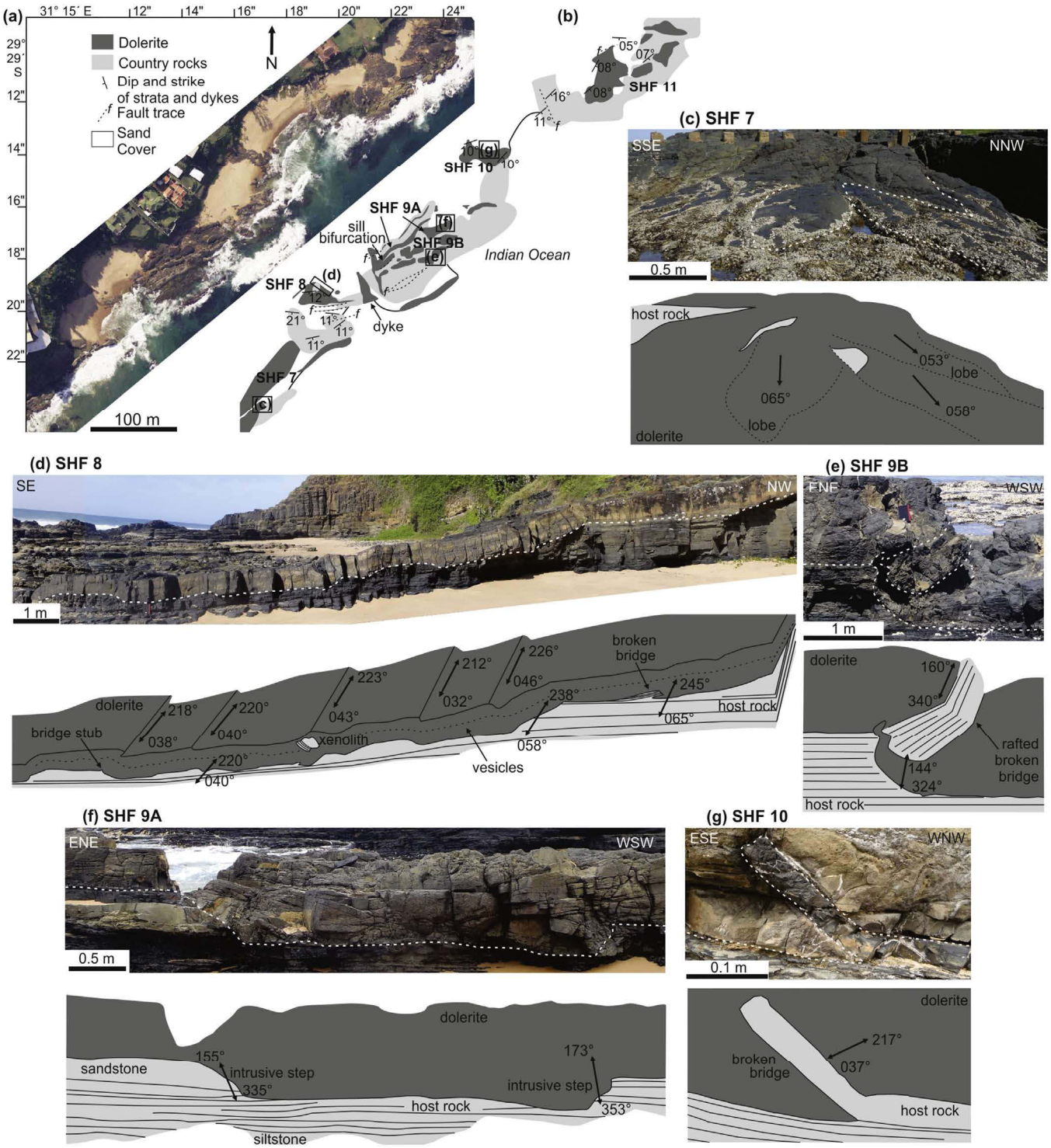

Fig. 5. (a) Aerial photograph and (b) geological map of northern Sheffield Beach. (c) ENE-trending magma lobes are preserved along the upper contact of SHF7. (d) SHF8 has several NE-SW oriented bridge structures along the lower and upper contacts. (f) A broken bridge along the lower contact of SHF9B has been detached by a magma horn. (f) Two intrusive steps occur along the lower contact of SHF9A oriented ~ NNW-SSE. (g) A NE-SW oriented broken bridge along the lower contact of SHF10.

cases, lineations are not representative of magma flow directions, as the *K*1 orientation is shown to be unrelated to the magmatic lineation (Callot and Guichet, 2003; Henry, 1997; Launeau and Cruden, 1998; Archanjo et al., 2012). Geoffroy et al. (2002) showed that the imbrication of the magnetic foliation could be used to imply magma flow directions instead of the lineation. Ellipsoid shapes derived from either a SPO or an AMS fabric are therefore critical when using them as magma flow indicators, especially with oblate-shaped fabrics (Callot and Guichet, 2003; Launeau and Cruden, 1998). If an ellipsoid is prolate, the fabric will be best defined by the lineation. However, the long and intermediate axes of strongly oblate fabrics are almost equal in length and can become inverted, consequently the foliation could define these fabrics (*e.g.* Geoffroy et al., 2002; Archanjo et al., 2012).

5. Results

5.1. Petrography

The sills comprise approximately 50% plagioclase, 45% clinopyroxene, 5% magnetite and/or pyrrhotite, and chlorite (replacing clinopyroxene) and biotite accessorily. Texturally the dolerites are sub-ophitic and variolitic, with occasional glomeroporphyritic textures. Minor interstitial devitrified glass is also present (*e.g.* ~25% in SHF8). Plagioclase is typically elongate but can vary from acicular to lath-like. Clinopyroxene is commonly stubby but is plumose in some finer-grained samples. Except for a few massive sills, most sills are vesicular and/or amygdaloidal.

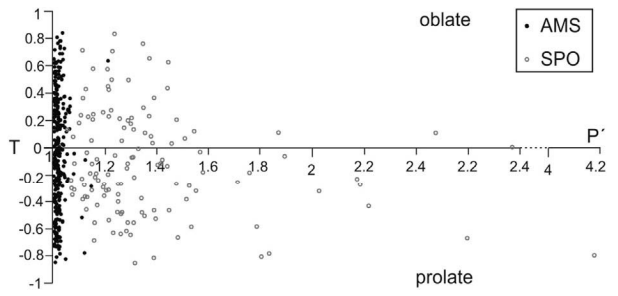

Fig. 6. Graphical illustration of the corrected degree of anisotropy (P′) and shape parameter (T) for AMS and SPO samples showing fabric shapes.

5.2. Field observations

The Thompson's Bay section of coastline hosts several sills (Fig. 3a and b) ranging in thickness from 1 m to 3 m (Table 1). Ropy-flow structures occur along the upper contact of TB1 plunging towards 215°, 217° and 240° (Fig. 3c). Elongated vesicles are dominant in the vesicular layer of TB2 plunging towards 301° (Fig. 3d) with one small ropy-flow structure preserved plunging towards 304° (Table 1). Along the upper contact of TB5, a small broken bridge structure is observed striking 307° (Fig. 3e). The upper contact of TB6 exhibits two coalesced magma lobes with terminations plunging towards 205° and 212° (Fig. 3f).

The sills from southern Sheffield Beach (Fig. 4a and b) range in thickness from 1 m to ~2.5 m (Table 1). SHF2 comprises a broken bridge and bridge stub on the upper and lower contacts respectively striking 004° (Fig. 4c). SHF3 is intruded into coarse sandstones, where two broken bridges have been preserved striking 064° and 243° (Fig. 4d). SHF4 is characterised by an intrusive step and scours along the upper sill contact striking 144° (Fig. 4e). SHF5 is a moderately dipping inclined sheet; a small broken bridge and a bridge stub, striking 354°, are observed along the upper contact (Fig. 4f). SHF6 is a sill intruded into an older dolerite sill with three small bridge structures, with variable strikes of 201°, 243° and 324°, along the southern lower sill contact (Fig. 4g). A large broken bridge, striking 041°, is present along the upper contact of SHF6 (Fig. 4a).

Several sills crop out along northern Sheffield Beach (Fig. 5a and b) from 0.5 m to >6 m in thickness (Table 1). Magma lobes crop out along the upper contact of SHF7 at the northern end of the sill, separated by sub-parallel raised edges all plunging towards 055°, 060° and 064° (Fig. 5c). SHF8 is characterised by a stepped morphology comprising several broken bridges and bridge stubs striking 212°–237° (Fig. 5d). SHF9 has a complicated morphology where the sill comprises two overlapping sill segments with a wedge of brecciated material separating the two. SHF9B is the

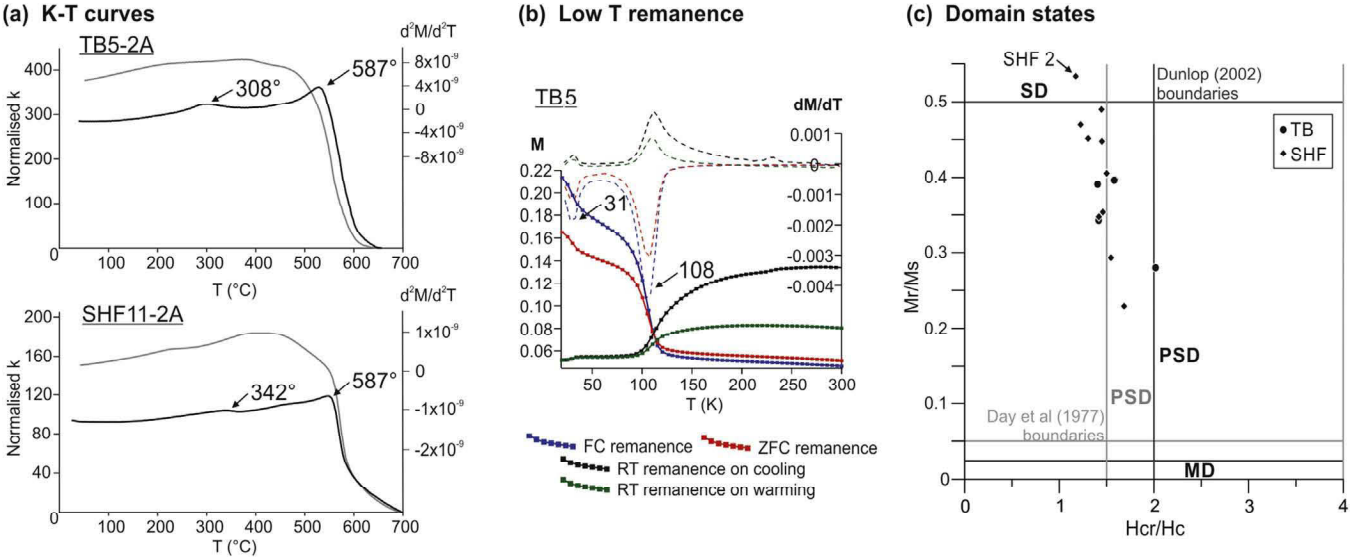

Fig. 7. Magnetic mineralogy results. (a) Susceptibility (K) versus temperature (T) curves, showing the heating curve (black) and cooling curve (grey) confirming the presence of magnetite; Curie temperatures of 587 °C (TB5) and 575 °C (SHF11) and pyrrhotite; Curie temperatures of 308 °C (TB5) and 342 °C (SHF11). (b) Thermomagnetic curves for TB from cooling and warming cycles yield unblocking temperatures of 31 K and 108 K representing pyrrhotite and magnetite respectively. (c) DCD plot with the Dunlop (2002) and Day et al. (1977) parameters showing a dominance of PSD grains.

upper magma segment and has two preserved parallel broken bridges striking 329° and 340° (Fig. 5e), SHF9A has three intrusive steps striking 325°, 343° and 346° (Fig. 5f). SHF10 has two parallel broken bridge structures preserved along the lower sill contact striking 211° and 220° (Fig. 5g). A small bridge stub occurs along the lower contact of SHF11 striking 325°.

5.3. Magnetic mineralogy

Thermomagnetic curves were used to infer the unblocking and Curie temperatures of the magnetic phases in the samples. Stoichiometric magnetite (Fe_3O_4) is the main magnetic component in all samples, yielding Curie temperatures between 575 °C and 590 °C (Fig. 7a) and unblocking temperatures of 110–120 K representative of the Verwey Transition of magnetite (Fig. 7b) (Verwey, 1939). Stoichiometric pyrrhotite (Fe_7S_8) occurs in nine of the 14 samples analysed, with a Curie temperature of ~320 °C (Fig. 7a) and an unblocking temperature of 30–35 K (Rochette et al., 1990). DC-Demagnetisation plots using the Day et al. (1977) and Dunlop (2002) parameters exhibit an overall PSD grain size, except for sample SHF2, which is SD (Fig. 7c). [See supplementary data for full results].

5.4. Fabric results

The average bulk susceptibility of the intrusions is 4150 × 10^{-6} SI, ranging from 606 × 10^{-6} SI to 10,100 × 10^{-6} SI (Table 1). P′ ranges from 1.003 to 1.057 with an average value of 1.021, indicating the AMS results are weakly anisotropic (Fig. 6). The average T = −0.033 with an almost neutral shape, with 54% negative T values. The long axes of the fabrics are generally shallowly dipping, the average angle between the fabric and the sill contact is 27° (disregarding data from three contacts having near vertical *K*1 axes.

For the SPO ellipsoids, the average P′ = 1.364 ranging from P′ = 1.053 to P′ = 2.773 with an outlier value of 4.128 (Table 2) (Fig. 6). The average T = −0.113 showing a weakly prolate shape (Fig. 6). The average angle between the long axes of the ellipsoid and the sill margin is moderately inclined at 45°.

5.4.1. Fabrics of the Thompson's Bay sills

The results for the AMS analyses of the Thompson's Bay sills are well constrained "normal" fabrics whereas the SPO results have large errors and wide spread data when represented stereographically (Fig. 8a). This trend is evident when the results are plotted on outcrop maps of the sills (Fig. 8b). Here the AMS results are consistent and predominantly parallel to one another. The results for TB1 show a strong correlation to the orientation of the ropy-flow structures with the AMS fabrics paralleling these structures, orientated 218°. Three sections of TB2 were sampled, the SPO of the three layers are sub-parallel plunging towards the NNW. The AMS fabrics are parallel and plunge shallowly towards the SSE (Fig. 8a). These fabrics are asymmetrical and differ in orientation to the elongated vesicles in the vesicular layer. The TB5 AMS results plunge towards the west and differ in orientation to the poorly constrained SPO. Although well constrained, the AMS fabrics and SPO are not parallel with the broken bridge long axis (Fig. 8). The few results obtained from TB6 show a perpendicular relationship with the magma lobes where the AMS fabrics plunge towards 306°. No SPO results were obtained for this sill.

5.4.2. Fabrics of the Sheffield Beach sills

As with the results from Thompson's Bay, the AMS fabrics for the Sheffield Beach sills are more rigorously constrained and yield smaller error ellipses than the SPO results (Fig. 9). SPO and AMS results from SHF2 are coaxial and plunge parallel to the bridge structures towards ~172° (Fig. 9), this is particularly evident with the AMS samples proximal to the bridge structure (Fig. 10). The AMS fabrics from SHF3 are asymmetrical across the contacts plunging towards the SW, coaxial with the bridge structures

Table 2
Shape Preferred Orientation results of plagioclase grains from Thompson's Bay and Sheffield Beach.

Sill	Contact	n	√F	*L*1	*L*2	*L*3	Foliation	P′	T	Grains
				dec/incl	dec/incl	dec/incl				
TB1	Upper	11	11.7%	244°/03°	335°/16°	144°/73°	234°/17°	1.100	−0.332	48,162
TB2	Upper	8	8.6%	349°/39°	215°/40°	101°/25°	191°/65°	1.132	−0.429	47,526
	Vesicular	3	14.0%	346°/45°	253°/03°	160°/45°	250°/45°	1.461	−0.482	12,786
	Lower	4	14.6%	285°/21°	020°/12°	137°/63°	227°/25°	1.253	0.504	13,733
TB5	Upper	4	8.3%	282°/04°	012°/04°	143°/85°	233°/05°	1.085	0.096	31,803
	Lower	4	7.6%	161°/01°	070°/53°	252°/37°	342°/53°	1.173	−0.233	23,697
SHF2	Upper	4	8.0%	161°/76°	254°/01°	344°/14°	074°/76°	1.179	−0.270	22,320
	Lower	5	11.1%	123°/23°	236°/32°	000°/42°	090°/48°	1.217	−0.345	31,520
SHF3	Upper	4	11.3%	130°/08°	037°/20°	240°/68°	330°/22°	1.134	−0.219	20,011
	Lower	4	12.8%	020°/51°	110°/00°	200°/39°	020°/51°	1.106	−0.042	16,552
SHF4	Upper	4	10.1%	001°/34°	120°/36°	241°/36°	331°/54°	1.140	−0.202	30,811
	Lower	2	7.9%	152°/45°	268°/24°	017°/36°	107°/55°	1.090	−0.215	16,203
SHF5	Upper	3	8.0%	308°/45°	104°/43°	205°/12°	295°/78°	1.143	−0.914	18,310
	Lower	2	6.1%	104°/53°	262°/35°	000°/11°	090°/79°	1.231	−0.484	9907
SHF6	Upper	6	7.0%	262°/22°	148°/46°	010°/36°	100°/54°	1.085	0.667	38,966
	Lower	5	7.2%	085°/30°	212°/46°	336°/29°	066°/61°	1.129	0.357	29,233
SHF7	Upper	4	8.3%	260°/27°	352°/04°	090°/63°	180°/27°	1.080	0.051	15,207
	Lower	3	7.7%	207°/38°	233°/29°	117°/38°	207°/52°	1.063	0.963	22,254
SHF8	Upper	3	5.1%	000°/12°	259°/41°	102°/47°	192°/44°	1.088	−0.344	20,743
	Lower	4	8.9%	320°/40°	147°/50°	053°/03°	143°/87°	1.236	0.213	20,765
SHF9A	Upper	2	9.5%	339°/24°	235°/29°	102°/51°	192°/39°	1.534	−0.167	5922
	Lower	1	4.8%	135°/42°	335°/47°	234°/10°	324°/80°	1.339	−0.273	4549
SHF9B	Lower	5	9.2%	047°/21°	197°/66°	313°/11°	043°/79°	1.138	0.009	17,425
SHF10	Upper	3	6.7%	083°/39°	233°/47°	340°/15°	070°/75°	1.115	0.382	11,737
	Lower	3	8.3%	151°/20°	060°/06°	315°/69°	042°/21°	1.204	0.429	10,782
SHF11	Upper	3	5.7%	213°/06°	121°/18°	319°/71°	049°/19°	1.140	0.146	12,857
	Lower	4	8.3%	069°/24°	334°/11°	221°/63°	311°/27°	1.158	−0.376	14,969

(Fig. 10). The SPO are poorly constrained and plunge asymmetrically towards the NE (Fig. 9). The AMS fabrics from SHF4 are symmetrical with the upper contact plunging towards 323° (Fig. 9), parallel to the long axis of the intrusive step (Fig. 10). The SPO for SHF4 is poorly constrained showing significant errors (Fig. 9) and a weak relationship with the orientation of the intrusive step (Fig. 10). The SHF5 upper and lower contact AMS results are well constrained, plunging asymmetrically towards the south (Fig. 9),

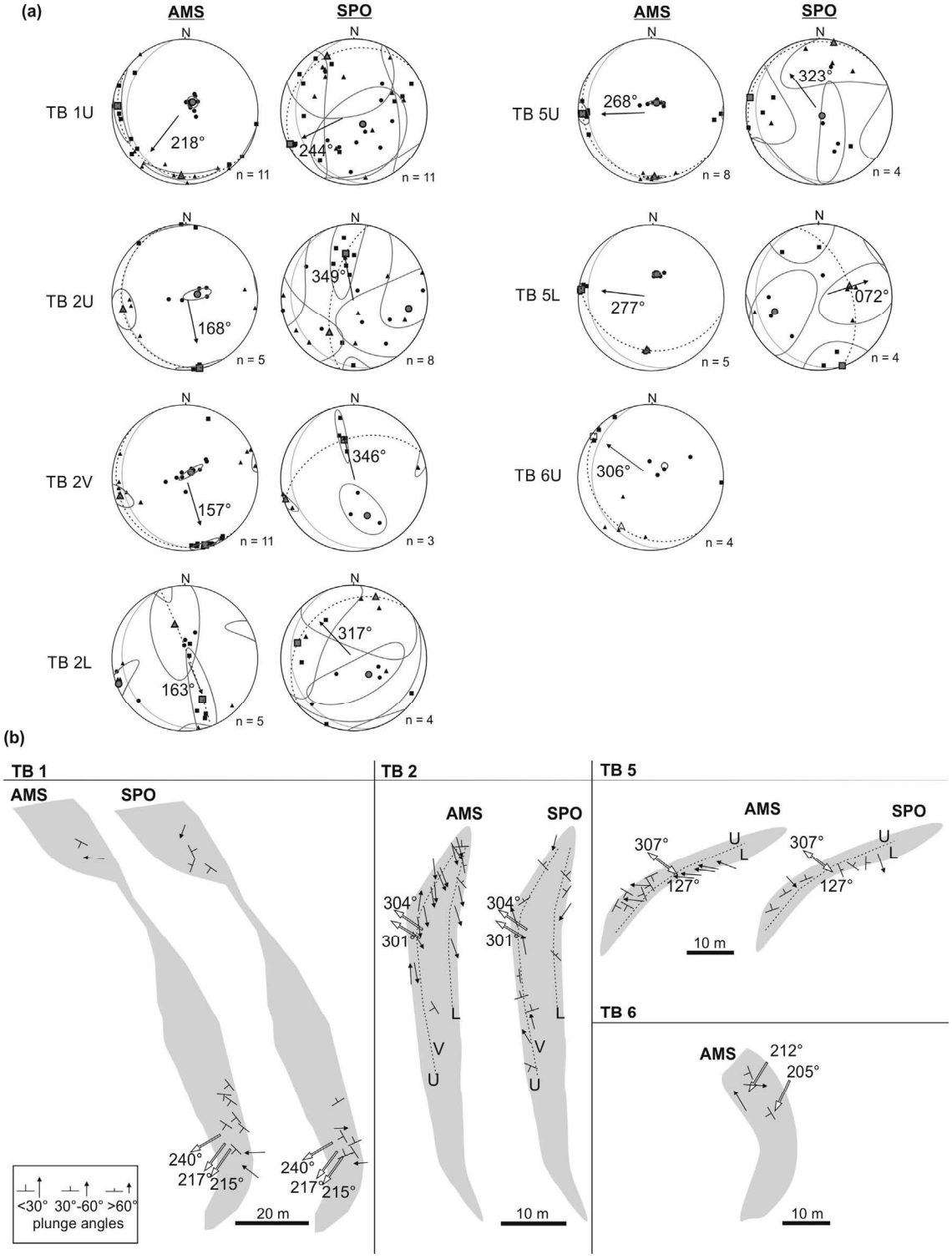

Fig. 8. (a) Stereographic projections of the AMS and SPO results for the upper (U) and lower (L) sill contacts for the sills from Thompson's Bay. TB2V is the discrete layer comprising elongated vesicles. For the AMS and SPO stereonets; squares = *K*1/*L*1, triangle = *K*2/*L*2, circle = *K*3/*L*3, average values are filled shapes with grey ellipses showing errors. Dashed great circles represent the foliation. Grey great circles represent the sill orientation. (b) Outcrop maps of the Thompson's Bay sills showing sample locations, results are represented by a dip and strike symbol (foliation) for oblate-shaped fabrics and arrows (lineation) for prolate-shaped fabrics. The white arrows represent the long axes of the magma flow indicators.

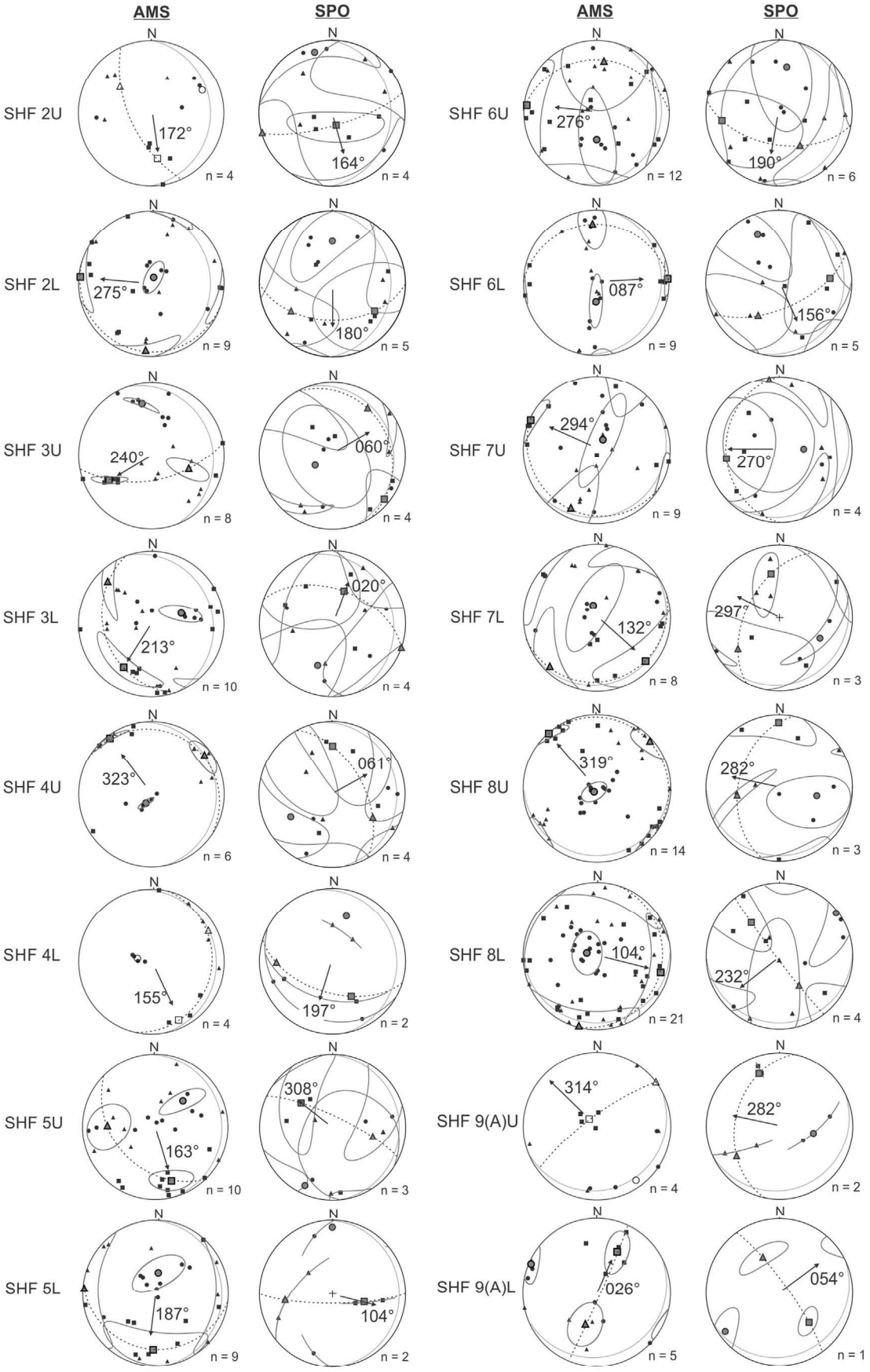

Fig. 9. Stereographic projections of the AMS and SPO results for the upper (U) and lower (L) sill contacts for the sills from Sheffield Beach. For the AMS and SPO stereonets; squares = *K*1/*L*1, triangle = *K*2/*L*2, circle = *K*3/*L*3, average values are filled shapes with grey ellipses showing errors. Dashed great circles represent the foliation. Grey great circles represent the sill orientation.

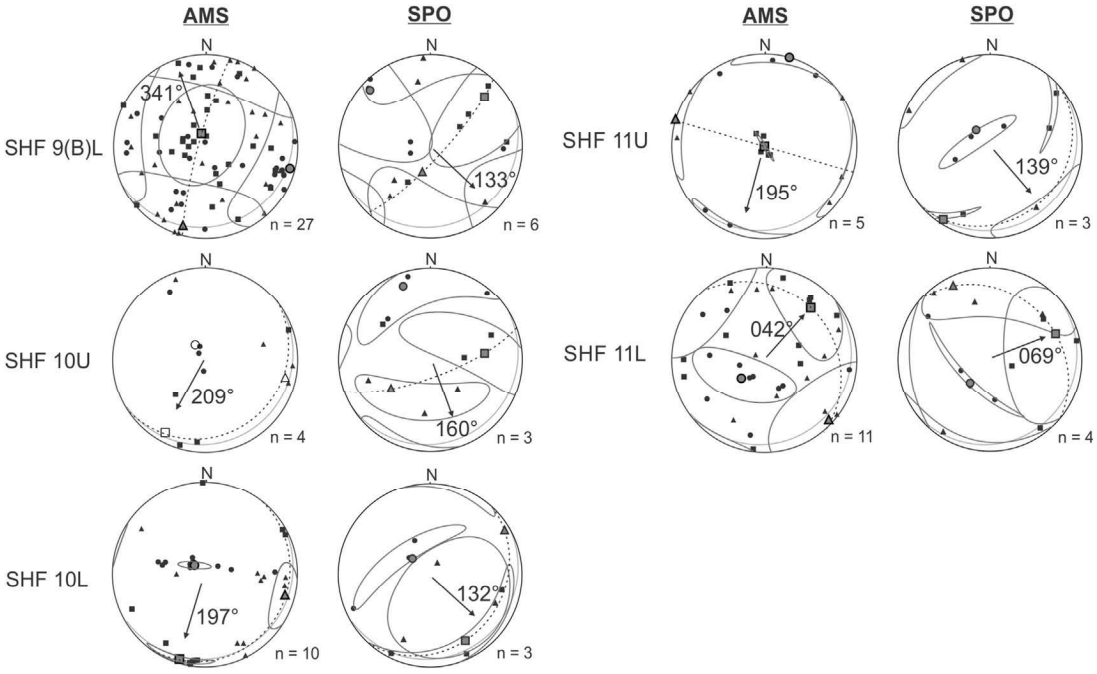

Fig. 9. (*continued*).

parallel to the bridge structures, particularly along the upper contact (Fig. 10). Few SPO results were obtained for SHF5 and are thus poorly constrained and dissimilar to the AMS fabrics and bridge structure long axes, plunging symmetrically towards the NW. The samples from SHF6 yielded symmetrical AMS fabrics, plunging towards the west, and poorly constrained SPO. There are no apparent relationships between the fabrics and the spread of orientations of the magma flow indicators (Fig. 10).

Symmetrical AMS fabrics were determined for SHF7 where the resultant fabrics plunge towards 294°, sub-parallel to the poorly constrained SPO (Fig. 9). These fabrics are perpendicular to the long axes of the magma lobes (Fig. 10). The well constrained AMS fabrics from SHF8 plunge symmetrically towards 319°, perpendicular to the numerous ~220° oriented bridge structures along the sill contacts (Fig. 10). This perpendicular relationship is mirrored by the few SPO results, which are steeply inclined and poorly constrained. The AMS fabrics from SHF9 are sub-vertical fabrics, the steeply inclined fabrics from the upper contact of SHF9A plunge towards 314° similar to the NW-oriented intrusive steps along the contact (Fig. 10). Although the errors from the AMS fabrics for SHF9B are significant, the fabrics plunge parallel to the bridge structures (Fig. 10). The SPO for all contacts of SHF9 are widely distributed and poorly constrained. Plunging asymmetrically towards 209°, the AMS fabrics from the contacts of SHF10 are coaxial with the long axes of the bridge structures (Figs. 9 and 10), the SPO fabrics plunge obliquely to the AMS fabrics and bridge structures, plunging towards the SE. The AMS fabrics from SHF11U plunge vertically, and the lower contact results plunge shallowly towards the NE. These results differ from the SPO, which plunge obliquely between the contacts (Figs. 9 and 10).

6. Discussion

6.1. Fabrics as magma flow indicators

Understanding how fabrics form requires knowledge of the timing of fabric formation and the regional setting. Fabrics that form during the last stages of magma intrusion preserve the final increment of strain. Melt viscosity plays a crucial role in the formation and preservation of crystal fabrics in intrusive igneous rocks. Whether the magma is a Binghamian or Newtonian liquid, imbricating crystals may develop along the sill contacts as a result of crystal movement in rigid-body rotation from magma flow (Fernández and Gasquet, 1994; Féménias et al., 2004). If the magma has not been subjected to particle reorganisation, for example flattening due to the overburden, the preserved fabric may indicate the direction of magma flow. The textures observed in the sills here appear to be magmatic in origin with no evidence of regional deformation, metamorphism, magma chamber processes or post-emplacement processes. The orientations of the fabrics, and the lack of abnormal fabrics within the sills, are varied enough that flattening has had little effect on the fabrics (Cañón-Tapia and Chavez-Alvarez, 2004). It follows that the preserved fabrics have formed as a result of internal processes and are a product of magma strain (Nicolas, 1992). The fabrics obtained from the SPO and AMS analyses may thus act as proxy for magma flow in the sills. However, the large differences in the orientation of the results obtained from the two methods would suggest otherwise. The majority of the AMS fabric data are “normal” fabrics suggesting that the AMS signature is likely a product of the magnetite PSD grain shape, as indicated by thermomagnetic analyses. The normal AMS fabrics represent the magnetite grain shape, it follows that these AMS shape fabrics are accurate proxies for magma flow directions. The SPO data are not constrained to the same degree as the AMS data with significant errors for the fabrics along the contacts. This variability in results between the two techniques seems to be related to the wide spread in orientations of the plagioclase SPO. Similar situations have been observed by Archanjo and Launeau (2004), however the SPO results were used to define the magmatic fabric as the AMS fabrics were interpreted as not representative of magma flow. Differences in the results here may be inherent of the method accuracy. Alternatively, the crystallisation of magnetite subsequent to plagioclase allows the plagioclase laths to be rotated during the final stages of magma flow. This

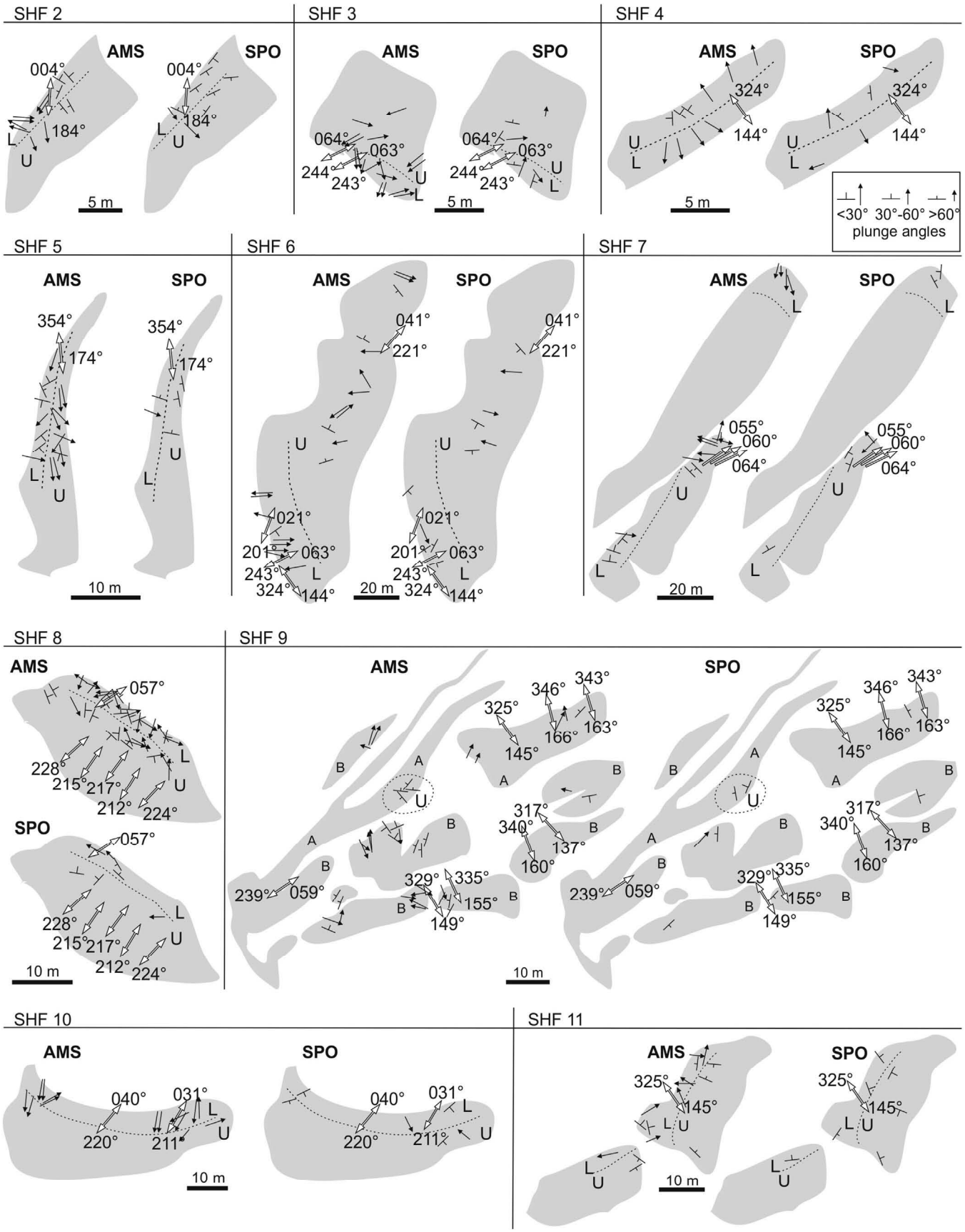

Fig. 10. Outcrop maps of the Sheffield Beach sills showing sample locations, results are represented by a dip and strike symbol (foliation) for oblate-shaped fabrics and arrows (lineation) for prolate-shaped fabrics. Dashed lines separate the samples from the upper (U) and lower (L) contacts. The white arrows represent the long axes of the magma flow indicators.

rotation may be responsible for the steep plagioclase fabrics along the contacts, at 45° from the sill contact, compared to 27° for the AMS fabrics. Due to the poorly constrained nature of SPO and the well constrained AMS fabrics, it would appear that in this case, the SPO results are not the most reliable indicators of magma flow in these sills.

6.2. Asymmetrical fabrics across contacts

In order to infer the magma flow direction, the sill contacts should ideally show symmetrical fabrics. Instead, some contacts exhibit asymmetrical fabrics for both AMS and SPO results. Symmetrical fabrics are the result of pure magma flow dynamics, where crystals become imbricated symmetrically along the upper and lower sill contacts. When an element of simple shear is introduced along the intrusion plane, the fabrics may become asymmetrical (Correa-Gomes et al., 2001). Increasing the amount of simple shear will affect the degree of anisotropy of the resulting fabrics, either increasing or decreasing the P′ when comparing the two contacts (Correa-Gomes et al., 2001; Féménias et al., 2004; Clemente et al., 2007). Where asymmetrical relationships exist in these sills, the P′ is comparable between the two contacts, thus it appears that the asymmetry is not a result of significant amount of simple shear, as this would have affected the shape anisotropy of the fabrics (Table 1). As most work done on asymmetrical fabrics has been conducted on vertical dykes (*e.g.* Correa-Gomes et al., 2001; Féménias et al., 2004; Clemente et al., 2007), perhaps the asymmetrical relationships observed in the fabrics here are the result of small-scale simple shear along lower sill contacts during magma intrusion. If this is the case, the imbrication of the crystals along the upper contacts could still be used to infer magma flow directions.

6.3. Fabric correlations with magma flow indicators

Many of these sills exhibit similarities between the shape fabrics and the implied direction of magma flow, with the AMS fabrics used as good indicators of magma flow directions. The ropy-flow structures observed below the upper contact of TB1 favourably correlate with the SPO and AMS fabrics throughout the intrusion, implying an accuracy in predicting magma flow. However, the elongated vesicles in the vesicular zone of TB2 and the fabric data do not present such a correlation: their fabrics differ in orientation to the elongated vesicles ~30°. This discrepancy may be due to the trapping of vesicles within discrete layers of the sill and not along the uppermost sill contact, as is the case in TB1. Due to the layered nature of the intrusion the vesicles may also have deformed against a more viscous material, hence preferentially preserving a remnant flow.

The sill SHF4 exhibits a large intrusive step where AMS fabrics are parallel with the orientations of the steps and magma injection scours. Along the lower contact of SHF9A in proximity to the three small intrusive steps, the AMS fabrics have similar orientations to the steps although these data are limiting. Overall, the match of these fabrics with the long axes of the intrusive steps implies that these structures are accurate indicators of magma flow directions.

For seven out of the nine sills sampled that had bridge structures, the fabrics were found to be parallel to the bridge long axes and thus consistent with the magma flow direction. The sills that do not have this relationship are SHF6 and SHF8. SHF6 shows varying orientations with respect to the preserved magma flow indicators. However, in SHF8 the measured fabrics are perpendicular to the field structures, a peculiarity attributed to several small originally isolated sill segments coalescent into a larger intrusion and creating numerous bridge structures (Fig. 11). This pattern is mimicked in the magma lobes observed along the upper contacts of TB6 and SHF7. Here the fabrics were found to be perpendicular to the long axes of these structures. As the samples were obtained away from the lobe terminations, it follows that these fabrics are not a result of flattening and instead could be from localised magma movement between the now merged lobes as they were incorporated into the main body of the intrusion, (Fig. 11).

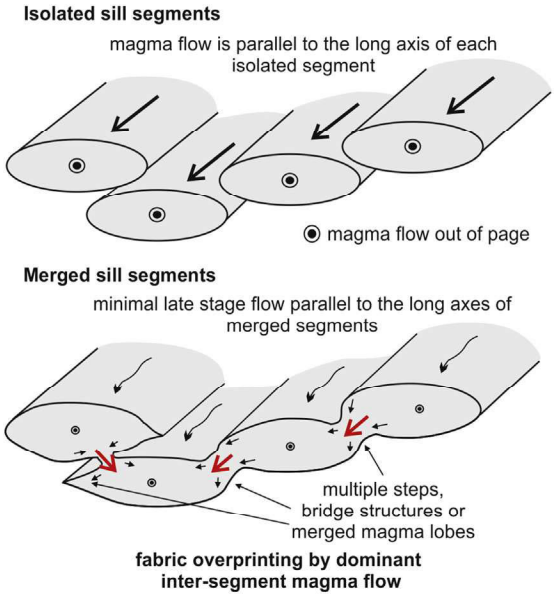

Fig. 11. Illustration of the coalescence of multiple sill segments showing the overprinting of the original magma flow direction (large black arrows) by the late-stage inter-segment magma flow (red arrows) with chaotic fabrics between segments indicating late-stage fabric overprinting (small black arrows). (For interpretation of the references to colour in this figure legend, the reader is referred to the web version of this article.)

6.4. Implications for inferring magma flow directions in sills

Where sills show individual or isolated structures across the intrusion, migration of magma between these segments would be minimal, therefore the fabrics throughout the sill should preserved initial magma flow directions. However, where several segments in close proximity merge to form one sill, a late-stage inter-segment magma flow overprints the original fabric pattern which was produced during the original magma intrusion phase (Fig. 11). Magee et al. (2013, 2016a) show that through the merging of magma segments with slightly different viscosities and melt characteristics, a result of xenolith entrainment, these sill segments become compartmentalised where the magma flow is contained within these partitioned sill zones. This process forms complex magma flow patterns in three dimensions and the fabrics obtained along the segments boundaries do not indicate the primary magma flow direction (Magee et al., 2013, 2016a). The isolation of magma flow within individual sill segments could have caused the resultant perpendicular fabrics. However, the majority of the samples were not obtained in close proximity to the magma flow indicators. The fabrics are thus most likely representative of flow from one segment towards another. The possibility of compartmentalisation is not ruled out, but confirms the complexity of magma flow dynamics within thin sills comprising multiple merged segments.

Caution should be taken when inferring magma flow directions from fabric data when obtained from intrusions comprising multiple merged segments. The various magma flow indicators studied here are accurate indicators of magma flow, as such these structures should be relied upon to indicate the initial magma

propagation direction. This is particularly true when inferring a magma source, as the initial magmatic foliation may later be overprinted by late-stage inter-segment magma migration.

7. Conclusions

Fabrics were acquired from sill contacts and compared with the implied magma flow directions obtained from field structures. The magnetic signatures responsible for the AMS results are dominated by well-constrain PSD-magnetite normal fabrics likely reflective of magma flow processes. The plagioclase SPO are generally steeply inclined, poorly constrained fabrics. The correlation of the SPO and AMS results is weak, likely due to the sporadic nature of the SPO data. Both techniques produced several asymmetrical fabrics with the upper contact data used to indicate magma flow directions. Magma flow indicators observed are largely the result of numerous sill segments merging to form continuous sheets. It can be concluded that the field structures (ropy-flow structures, intrusive steps, magma lobes and bridge structures) successfully predict magma flow directions in sills. Where fabrics are perpendicular to these structures, late-stage magma flow between the merged segments is considered to have overprinted the initial magma intrusion direction.

Acknowledgements

L. Hoyer acknowledges a Visiting Research Fellowship from the Institute for Rock Magnetism at the University of Minnesota and thanks Dario Bilardello and Mike Jackson for their help whilst visiting the IRM. Thanks to Patrick Launeau for his assistance with the SPO-2003 programme. The authors would like to thank Craig Magee and Jean-Luc Bouchez for their constructive remarks, and Sven Morgan, Marcos Egydio-Silva and an anonymous reviewer for comments on a previous manuscript. The authors acknowledge Mukesh Seyambu (University of KwaZulu-Natal) for assistance with thin section preparation. L. Hoyer would like to thank S. Aberdeen, K. Benallack, D. Cousins, A. Krebs, K. Ridgeway, L. Salzmann, J. Weitz and E. Wiles for their assistance during drilling. L. Hoyer acknowledges a free-standing NRF Scarce Skills Scholarship.

Appendix A. Supplementary data

Supplementary data related to this article can be found at http://dx.doi.org/10.1016/j.jsg.2017.02.005.

References

Archanjo, C.J., Launeau, P., 2004. Magma flow inferred from preferred orientations of plagioclase of the Rio Ceará-Mirim dyke swarm (NE Brazil) and its AMS significance. In: Martín-Hernández, F., Luneberg, C.M., Aubourg, C., Jackson, M. (Eds.), Magnetic Fabric: Methods and Applications, vol. 238. Geological Society of London Special Publication, pp. 285–298.

Archanjo, C.J., Campanha, G.A.C., Salazar, C.A., Launeau, P., 2012. Using AMS combined with mineral shape preferred orientation to understand the emplacement fabrics of the Apiaí gabbro-norite (Ribeira Belt, SE Brazil). Int. J. Sci. 101, 731–745.

Aubourg, C., Tshoso, G., Le Gall, B., Bertrand, H., Tiercelin, J.-J., Kampunzu, A.B., Dyment, J., Modisi, M., 2008. Magma flow revealed by magnetic fabric in the Okavango giant dyke swarm, Karoo igneous province, northern Botswana. J. Volcanol. Geotherm. Res. 170, 247–261.

Blanchard, J.-P., Boyer, P., Gagny, C., 1979. Un nouveau critere de sens de mise en place dans une caisse filonienne: le “pincement” des mineraux aux epontes: orientation des minéraux dans un magma en écoulement. Tectonophysics 53, 1–25.

Callot, J., Guichet, X., 2003. Rock texture and magnetic lineation in dykes: a simple analytical model. Tectonophysics 366, 207–222.

Callot, J., Geoffroy, L., Aubourg, C., Pozzi, J., Mege, D., 2001. Magma flow directions of shallow dykes from the East Greenland volcanic margin inferred from magnetic fabric studies. Tectonophysics 335, 313–329.

Cañón-Tapia, E., 2004. Anisotropy of magnetic susceptibility of lava flows and dykes: a historical account. In: Martín-Hernández, F., Luneberg, C.M., Aubourg, C., Jackson, M. (Eds.), Magnetic Fabric: Methods and Applications, vol. 238. Geological Society of London Special Publication, pp. 1–7.

Cañón-Tapia, E., Chávez-Álvarez, M.J., 2004. Theoretical aspects of particle movement in flowing magma: implications for the anisotropy of magnetic susceptibility in dykes. In: Martín-Hernández, F., Luneberg, C.M., Aubourg, C., Jackson, M. (Eds.), Magnetic Fabric: Methods and Applications, vol. 238. Geological Society of London Special Publication, pp. 227–249.

Correa-Gomes, L.C., Souza Filho, C.R., Martins, C.J.F.N., Oliviera, E.P., 2001. Development of symmetrical and asymmetrical fabrics in sheet-like igneous bodies: the role of magma flow and wall-rock displacements in theoretical and natural cases. J. Struct. Geol. 23, 1415–1428.

Clemente, C.S., Amorós, E.B., Crespo, M.G., 2007. Dike intrusion under shear stress: effects on magnetic and vesicle fabrics in dikes from rift zones of Tenerife (Canary Islands). J. Struct. Geol. 29, 1931–1941.

Day, R.M., Fuller, M., Schmidt, V.A., 1977. Hysteresis properties of titanomagnetites: grain size and composition dependence. Phys. Earth Planet. Interiors 13, 260–267.

Dunlop, D.J., 2002. Theory and application of the Day plot (M_{rs}/M_s versus H_{cr}/H_c): 2. Application to data for rocks, sediments and soils. J. Geophys. Res. 107 (B3), 2057. http://dx.doi.org/10.1029/2001JB000487.

Ellwood, B.B., 1978. Flow and emplacement direction determined for selected basaltic bodies using magnetic susceptibility anisotropy measurements. Earth Planet. Sci. Letters 41 (3), 1270–1273.

Erlank, A.J., 1984. Petrogenesis of the volcanic rocks of the Karoo province. Geol. Soc. S. Afr. Special Publ. 13, 395.

Féménias, O., Diot, H., Berza, T., Gauffriau, A., Demaiffe, D., 2004. Asymmetrical to symmetrical magnetic fabric of dikes: paleo-flow orientations and paleo-stresses recorded on feeder-bodies from the Motru Dike Swarm (Romania). J. Struct. Geol. 26, 1401–1418.

Fernández, A.N., Gasquet, D.R., 1994. Relative rheological evolution of chemical contrasted coeval magmas: example of the Tichka plutonic complex (Morocco). Contrib Mineral. Petrol. 116, 316–326.

Ferré, E.C., Bordarier, C., Marsh, J.S., 2002. Magma flow inferred from AMS fabrics in a layered mafic sill, Insizwa, South Africa. Tectonophysics 354, 1–23.

Fink, J.H., Fletcher, R.C., 1978. Ropy pahoehoe: surface folding of a viscous fluid. J. Volcanol. Geotherm. Res. 4, 151–170.

Gay, N.C., 1966. Orientation of mineral lineation along the flow direction in rocks: a discussion. Tectonophysics 3, 559–564.

Gay, N.C., 1967. Pure shear and simple shear deformation of inhomogeneous viscous fluids. 1. Theory. Tectonophys. 5, 211–234.

Geoffroy, L., Callot, J.P., Aubourg, C., Moreira, M., 2002. Is the common use of AMS in mafic dykes scientifically correct? Terra Nova 14, 183–190.

Gil-Imaz, A., Pocoví, A., Lago, M., Galé, C., Arranz, E., Rillo, C., Guerrero, E., 2006. Magma flow and thermal contraction fabric in tabular intrusions inferred from AMS analysis. A case study in a late-Variscan folded sill of the Albarracı'n Massif (southeastern Iberian Chain, Spain). J. Struct. Geol. 28, 641–653.

Graham, J.W., 1954. Magnetic susceptibility anisotropy, an unexploited fabric element. Bull. Geol. Soc. Am. 65, 1257–1258.

Hastie, W.W., Aubourg, C., Watkeys, M.K., 2011. Significance of magnetic and petrofabric in Karoo-feeder dykes, northern Lebombo. Tectonophysics 513, 96–111.

Henry, B., 1997. The magnetic zone axis: a new element of magnetic fabric for the interpretation of magnetic lineation. Tectonophysics 271, 325–331.

Horsman, E., Tikoff, B., Morgan, S., 2005. Emplacement-related fabric and multiple sheets in the Maiden Creek sill, Henry mountains, Utah, USA. J. Struct. Geol. 27, 1426–1444.

Hoyer, L., Watkeys, M.K., 2015. Assessing SPO techniques to constrain magma flow: examples from sills of the Karoo Igneous Province, South Africa. Tectonophysics 656, 61–73.

Hutton, D.H.W., 2009. Insights into magmatism in volcanic margins: bridge structures and a new mechanism of basic sill emplacement – theron Mountains, Antarctica. Pet. Geosci. 15, 269–278.

Jelinek, V., 1978. Statistical processing of anisotropy of magnetic susceptibility measured on a group of specimens and its applications. Stud. Geophys. Geodyn. 22, 50–62.

Jourdan, F., Féraud, G., Bertrand, H., Kampunzu, A.B., Tshoso, G., Watkeys, M.K., Le Gall, B., 2005. Karoo large igneous province: brevity, origin and relation to mass extinction question by new $^{40}Ar/^{39}Ar$ age data. Geology 33, 745–748.

Jourdan, F., Féraud, G., Bertrand, H., Watkeys, M.K., Renne, P.R., 2007. Distinct brief major events in the Karoo large igneous province clarified by new $^{40}Ar/^{39}Ar$ ages on the Lesotho basalts. Lithos 98, 195–209.

Kattenhorn, S.A., Watkeys, M.K., 1995. Blunt-ended dyke segments. J. Struct. Geol. 17, 1535–1542.

Khan, M.A., 1962. Anisotropy of magnetic susceptibility of some igneous and metamorphic rocks. J. Geophys. Res. 67, 2873–2885.

Knight, M.D., Walker, G.P.L., 1988. Magma flow directions in dikes of the Koolau Complex, Oahu, determined from magnetic fabric studies. J. Geophys. Res. 93, 4301–4319.

Launeau, P., 2004. Mise en évidence des écoulements magmatiques par analyse d'images 2-D des distributions 3-D d'Orientations Préferentielles de Formes. Bull. Geol. Soc. France 175, 331–350.

Launeau, P., Cruden, A.R., 1998. Magmatic fabric acquisition mechanisms in a syenite: results of a combined anisotropy of magnetic susceptibility and image analysis study. J. Geophys. Res. 103, 5067–5089.

Launeau, P., Robin, P.-Y.F., 1996. Fabric analysis using the intercept method.

Tectonophysics 267, 91–119.
Launeau, P., Robin, P.-Y.F., 2005. Determination of fabric and strain ellipsoids from measured sectional ellipses—implementation and applications. J. Struct. Geol. 27, 2223–2233.
Liss, D., Hutton, D.H.W., Owens, W.H., 2002. Ropy flow structures: a neglected indicator of magma-flow direction in sills and dikes. Geology 30, 715–718.
Loock, S., Diot, H., Van Wyk de Vries, B., Launeau, P., Merle, O., Vedboin, F., Petronis, M.S., 2008. Lava flow internal structure found from AMS and textural data: an example in methodology form the Chaîne des Puys, France. J. Volcanol. Geotherm. Res. 177, 1092–1104.
Maes, S.M., Férre, E.C., Tikoff, B., Brown, P.E., Marsh, J.S., 2008. Rock magnetic stratigraphy of a mafic layered sill: a key to the Karoo volcanics plumbing system. J. Volcanol. Geotherm. Res. 172, 75–92.
Magee, C., Stevenson, C.T.E., O'Driscoll, B., Petronis, M.S., 2012. Local and regional controls on the lateral emplacement of the ben hiant dolerite intrusion, Ardnamurchan (NW scotland). J. Struct. Geol. 39, 66–82.
Magee, C., O'Driscoll, B., Petronis, M.S., Stevenson, C.T.E., Clay, P.L., Gertisser, R., 2013. Magma Rheology Variations in Sheet Intrusion of the Ardnamurchan Central Complex (Scotland) Inferred from Gabbro Inclusion Characteristics.
Magee, C., O'Driscoll, B., Petronis, M.S., Stevenson, C.T.E., 2016a. Three-dimensional magma flow dynamics within subvolcanic sheet intrusions. Geosphere 12, 842–866.
Magee, C., Muirhead, J.D., Karvelas, A., Holford, S.P., Jackson, C.A.L., Bastow, I.A., Schofield, N., Stevenson, C.T.E., McLean, C., McCarthy, W., Shtukert, O., 2016b. Lateral magma flow in mafic sill complexes. Geosphere 12, 809–841.
Morgan, S., Stanik, A., Horsman, E., Tikoff, B., de Saint Blanquat, M., Habert, G., 2008. Emplacement of multiple magma sheets and wall rock deformation: trachyte Mesa intrusion, Henry Mountains, Utah. J. Struct. Geol. 30, 491–512.
Morris, G.A., Kamada, M., Martinez, V., 2008. Emplacement of the etive dyke swarm, scotland: implications of dyke morphology and AMS data. In: Thomson, K., Petford, N. (Eds.), Structure and Emplacement of High-level Magmatic Systems, vol. 302. Geological Society, London Special Publication, pp. 149–158.
Muirhead, J.D., Airoldi, G., Rowland, J.V., White, J.D.L., 2012. Interconnected sills and inclined sheet intrusions control shallow magma transport in the Ferrar large igneous province, Antarctica. Geol. Soc. Am. Bull. 124, 162–180.
Nicolas, A., 1992. Kinematics in magmatic rocks with special reference to gabbros. J. Petrol. 33, 891–915.
Nicholson, R., Ejiofor, I.B., 1987. The three-dimensional morphology of arrays of echelon and sigmoidal, mineral-filled fractures: data from north Cornwall. J. Geol. Soc. Lond. 144, 79–83.
Nicholson, R., Pollard, D.D., 1985. Dilation and linkage of echelon cracks. J. Struct. Geol. 7, 583–590.
Philpotts, A.R., Philpotts, D.E., 2007. Upward and downward flow in a camptonite dike as recorded by deformed vesicles and the anisotropy of magnetic susceptibility (AMS). J. Volcanol. Geotherm. Res. 161, 81–94.
Poland, M.P., Fink, J.H., Tauxe, L., 2004. Patterns of magma flow in segmented silicic dikes at Summer Coon volcano, Colorado: AMS and thin sections analysis. Earth Planet. Sci. Lett. 219, 155–169.
Pollard, D.D., 1987. Elementary fracture mechanics applied to the structural interpretation of dykes. In: Halls, H.C., Fahrig, W.F. (Eds.), Mafic Dyke Swarms, vol. 34, pp. 5–24. Geological Association of Canada Special Paper.
Pollard, D.D., Muller, O.H., Dockstader, D.R., 1975. The form and growth of fingered sheet intrusions. Geol. Soc. Am. Bull. 86, 351–363.
Rickwood, P.C., 1990. The anatomy of a dyke and the determination of propagation and magma-flow directions. In: Parker, A.J., Rickwood, P.C., Tucker, D.H. (Eds.), Mafic Dykes and Emplacement Mechanisms, vol. 2, pp. 81–100. Proceedings of the Second international dyke conference, Adelaide, South Australia.
Robin, P.-Y.F., 2002. Determination of fabric and strain ellipsoids from measured sectional ellipses – Theory. J. Struct. Geol. 24, 531–544.
Rochette, P., Fillion, G., Mattei, J.-L., Dekkers, M.J., 1990. Magnetic transition at 30 – 34 K in pyrrhotite: insight into a widespread occurrence of this mineral in rocks. Earth Planet. Sci. Lett. 98, 319–328.
Rochette, P., Jenatton, L., Dupuy, C., Boudier, F., Reuber, I., 1991. Diabase dikes emplacements in the Oman Ophiolite: a magnetic fabric study with reference to geochemistry. In: Peters, T., Nicolas, A., Coleman, R.G. (Eds.), Ophiolite Genesis and Evolution of the Oceanic Lithosphere. Kluwer, Dordrecht, pp. 55–82.
Rochette, P., Aubourg, C., Perrin, M., 1999. Is this magnetic fabric normal? A review and case studies in volcanic formations. Tectonophysics 307, 219–234.
Schofield, N., Heaton, L., Holford, S.P., Archer, S.G., Jackson, C.A.-L., Jolley, D.W., 2012a. Seismic imaging of 'broken bridges': linking seismic to outcrop-scale investigations of intrusive magma lobes. J. Geol. Soc. Lond. 169, 421–426.
Schofield, N., Brown, D.J., Magee, C., Stevenson, C.T., 2012b. Sill morphology and comparison of brittle and non-brittle emplacement mechanisms. J. Geol. Soc. Lond. 169, 127–141.
Stephenson, A., Sadikun, S., Potter, D.K., 1986. A theoretical and experimental comparison of the anisotropies of magnetic susceptibility and remanence in rocks and minerals. Geophys. J. Int. 84, 185–200.
Stevenson, C.T.E., Owens, W.H., Hutton, D.H.W., 2007. Flow lobes in granite: the determination of magma flow direction in the Trawenagh Bay Granite, northwestern Ireland, using anisotropy of magnetic susceptibility. Geol. Soc. Am. Bull. 119, 1368–1386.
Svensen, H., Corfu, F., Polteau, S., Hammer, Ø., Planke, S., 2012. Rapid magma emplacement in the Karoo large igneous province. Earth Planet. Sci. Lett. 325–326, 1–9.
Tarling, D.H., Hrouda, F., 1993. The Magnetic Anisotropy of Rocks. Chapman and Hall, London, p. 218.
Tauxe, L., Gee, J., Staudigel, H., 1998. Flow directions in dike from anisotropy of magnetic susceptibility data: the bootstrap way. J. Geophys. Res. 103, 17775–17790.
Thomson, K., Hutton, D., 2004. Geometry and growth of sill complexes: insights using 3D seismic from the North Rockall trough. Bull. Volcanol. 66, 362–375.
Verwey, E.J., 1939. Electron conduction of magnetite (Fe_3O_4) and its transition point at low temperature. Nature 144, 327–328.
Watkeys, M.K., 2006. The break-up of Gondwana: a south African perspective. In: Johnson, M.R., Anhaeusser, C.R., Thomas, R.J. (Eds.), The Geology of South Africa. Geological Society of South Africa, Council for Geoscience, pp. 531–539.